1   **Flood Risk Assessment and Increased Resilience for Coastal Urban**

2   **Watersheds under the Combined Impact of Storm Tide and Heavy Rainfall**

3   Yawen Shen[1], Mohamed M. Morsy[2,3], Chris Huxley[4], Navid Tahvildari[5], Jonathan L. Goodall[6,*]

4   [1]Graduate Research Assistant, Dept. of Engineering Systems and Environment, Univ. of Virginia, Olsson

5   Hall, Charlottesville, VA 22904-4742, USA. E-mail: ys5dv@virginia.edu

6   [2]Research Associate, Dept. of Civil and Environmental Engineering, Univ. of Virginia, Olsson Hall,

7   Charlottesville, VA 22904-4742, USA. E-mail: mmm4dh@virginia.edu

8   [3]Assistant Professor, Irrigation and Hydraulics Department, Faculty of Engineering, Cairo University,

9   P.O. Box 12211, Giza 12613, Egypt

10   [4]Senior Engineer, BTM WBM Pty Ltd, Level 8, 200 Creek Street, Brisbane, 4000, Australia. E-mail:

11   chris.huxley@tuflow.com

12   [5]Assistant Professor, Dept. of Civil and Environmental Engineering, Old Dominion University, Norfolk,

13   VA 23529. E-mail: ntahvild@odu.edu

14   [6]Associate Professor, Dept. of Engineering Systems and Environment, Univ. of Virginia, Olsson Hall,

15   Charlottesville, VA 22904-4742, USA. E-mail: goodall@virginia.edu

16

17   [*] corresponding author: E-mail: goodall@virginia.edu, phone: +1 (434) 243-5019

18   **Abstract**

19   Low-lying coastal cities are vulnerable to flooding under the combined impact of storm tide and heavy

20   rainfall. While storm tide or heavy rainfall alone is able to directly cause widespread flooding in coastal

21   areas, often heavy rainfall and storm tide happen concurrently, and the severity of flooding is greatly

22   exacerbated. Current methods for understanding flood risk and mapping floodplains normally does not

23   clearly communicate either the individual or combined impact of these two flooding mechanisms. Flood

24   mitigation strategies typically target either rainfall-driven flooding (e.g., stormwater controls) or tidally-

25   driven flooding (e.g., flood walls and tide gates). Thus, better understanding and communicating the

26   individual and combined flood risk resulting from these two mechanisms can be important to improving

27   flood resilience. To address this need, this study presents tools and methods for floodplain mapping in

28   coastal urban environments were rainfall and storm tide driven flooding can be better understood and

29   communicated. The approaches are demonstrated for a watershed in Norfolk, VA, USA as a case study

30   system using a 1D pipe/2D overland flow hydrodynamic model built for the watershed. Storm tide and

31   heavy rainfall events with return periods varying from 1 to 100-year were designed based on historical

32   observations and combined into a series of compound storm scenarios. Then these compound storm

33   scenarios were simulated using the hydrodynamic model for simulating flow through both the land

34   surface and underground pipe network systems. Results show how the capacity of the drainage system,

35   and therefore flood risk reduction, is sensitive to storm tide levels, even for less extreme events with a 1-

36   year return period. The model also provides new insights into the role of stormwater infrastructure in

37   exacerbating flooding risk within communities during high sea level conditions. Results demonstrate how

38   dividing the floodplain into different regions based on the dominate flooding mechanism (rainfall vs.

39   storm tide) makes it possible to better target mitigation strategies to improve flood resilience. To this end,

40   a transition zone index (TZI) is presented to help decision makers identify the change from rainfall-driven

41   to tide-driven flooding for locations within a watershed. Finally, we demonstrate how different flood

42   mitigation strategies can be tested using this modeling approach to better understand their impact on

43 increasing flood resilience within the system for portions of the floodplain impacted by rainfall-driven

44 and tidal-driven flooding.

45 **Author keywords:** Coastal City; Urban Hydrology; Coastal Flood Mapping; Storm Tide; Heavy

46 Rainfall; 2D Hydrodynamic Modeling; Flood Resilience

47

48 **1. Introduction**

49 In the context of sea level rise and climate change, flooding is one of the most challenging issues facing

50 coastal cities today (Hallegatte et. al., 2013; Woodruff et al., 2013). Coastal cities form a vital component

51 of national and global economies; however, coastal cities and their economies are increasingly vulnerable

52 to extreme storm events (Hanson et al., 2011). As a consequence of extreme storm events, flooding

53 impacts on these low-lying, densely populated, and highly developed regions can be devastating (Gallien

54 et al., 2014; Wahl et. al., 2015; Karamouz et al., 2017; Sadler et al., 2017; Bilskie and Hagen, 2018). In

55 coastal cities, flooding is primary caused by two processes: surface runoff due to inland heavy rainfall and

56 tidal flooding from extreme high tide (Dawson et al., 2008; Archetti et al., 2011; Xu et al. 2014; Wahl et.

57 al., 2015). Heavy rainfall is more likely to cause severe flooding in urban areas with poorly functioning or

58 insufficient stormwater infrastructure (Upadhyaya et. al., 2014; Yazdanfar and Sharma, 2015). In coastal

59 cities, rainfall-driven stormwater collected by drainage system is designed to drain into the sea either by

60 gravity-fed flow or pumping. However, during extreme high tide events, the drainage capabilities are

61 greatly reduced with a worse situation of backward flow. Additionally, extreme high tide alone is able to

62 directly cause widespread coastal flooding (Xu et. al., 2014; Castrucci and Tahvildari, 2018). Thus, if

63 heavy precipitation and extreme high tide happen concurrently, the severity of flood can be greatly

64 exacerbated (Zheng et al., 2013; Xu et al., 2014; Wahl et. al., 2015; Karamouz et al., 2015, 2017; Wu et

65 al., 2018). The extreme high tide discussed in this study is in the form of storm tide, which is the total

66 observed seawater level during a storm resulting from the combination of storm surge and the

67 astronomical tide.

68   Prior studies have used statistical methods to explore the interdependence between storm tide and

69   heavy rainfall and their combined impact on flood risk (Zheng et. al., 2013; Xu et al., 2014; Wahl et. al.,

70   2015; Batten et al., 2017; Wu et al., 2018). Zheng et al. (2013) investigated the presence of the

71   dependence between extreme rainfall and storm surge on Australian coastline using available rainfall and

72   tide level observations. They found a statistically significant dependence with regional and seasonal

73   variations for the majority of studied locations. Wahl et al. (2015) studied the likelihood of concurrent

74   storm tide and heavy rainfall for major coastal cities in the contiguous United States. It was found that the

75   probability of combined storms is higher for the Atlantic/Gulf coast relative to the Pacific coast.

76   Meanwhile, in many of the focused cities, the number of compound events has increased greatly over the

77   past century, and this trend may continue under the changing environment. Xu (2014) and Batten (2017)

78   estimated the joint probability of storm tide and extreme rainfall in their study areas and proposed design

79   guidance for future flooding preparedness. Specifically, Batten (2017), who worked on the same region,

80   coastal of Virginia, USA, as the current study, showed that over 50% of the rainfall events happened

81   when sea water level was higher than mean daily high tide. While statistical approaches are important for

82   understanding risk, they are not able to identify specific areas within a coastal community vulnerable to

83   flooding, nor are they able to quantify how modifications to the built environment, in the form of

84   infrastructure improvements, can mitigate flooding risk. Physical models of the system are needed for

85   these challenges.

86   Coupled one-dimension (1D) pipe and two-dimension (2D) overland flood models are an efficient

87   way to simulate urban flooding and have been widely used for assessing urban flood risk (Leandro et al.,

88   2009; Seyoum et al., 2012; Russo et al., 2015; Fan et al., 2017; Xu et al., 2017; Martins et al., 2018). In

89   prior studies, 1D models (Ray et. al., 2011; Lian et. al., 2013; Bacopoulos et al., 2017; Karamouz et al.,

90   2017) or 2D models (Karamouz et al., 2017; Silva-Araya et. al., 2017) have been used to investigate the

91   combined impact of storm tide and extreme rainfall, but the combination of 2D/1D modeling approaches

92   to simulate both overland flow and flow through stormwater drainage systems for coastal watersheds is

93   novel. Coastal regions are usually located in low-relief terrains with flat or mild slopes and a large amount

94   of storage potential, especially in coastal cities with complex topography and a large number of artificial

95   structures. Routing water in such regions is not as straightforward as in high-gradient regions since water

96   does not always stay within river channels. In confined channels, 1D models are able to generate good

97   estimation of flooding as long as the water remains in the channels (Marks et al., 2004; Leandro et al.,

98   2009). However, for extreme storm events in urban environment, stormwater flow can easily overtops the

99   curbs in the streets, and the direction of the flow may change dramatically. In such conditions, a 2D

100   model is a more reliable tool for urban flood simulation. However, even though 2D models were used in

101   Karamouz (2017) and Silva-Araya (2017), the underground drainage system was not considered in both

102   studies. Underground drainage system is a key component of stormwater management infrastructure in

103   coastal cities, and its efficiency could be greatly influenced by the downstream tidal boundary conditions

104   (Archetti at. al., 2011). Therefore, in order to simulate coastal city flooding in a realistic manner, flood

105   models need to be capable of simulating the dynamics of flow on ground surface and pipe flow in

106   underground drainage system, as well as the interaction between them. An effective way is to use a 1D

107   pipe and 2D overland coupled model. Several commercial or open-source 1D/2D modeling system are

108   available, such as, the Two-dimensional Unsteady Flow (TUFLOW) model (Syme, 2001), MIKE 21

109   (Carr and Smith, 2006), XP-SWMM, Leandro (2016), and Wu (2017). Such modeling systems can

110   support coastal flood mapping with the consideration of the individual and combined flood risk resulting

111   from storm tide and heavy rainfall, and it can be important to improving flood resilience by testing the

112   impact of different potential mitigation strategies.

113   In prior studies, geospatial information and hydrodynamic models have been used for

114   understanding flood risk and mapping coastal floodplains (Wang et al., 2002; Karamouz et al., 2015;

115   Karamouz et al., 2017; FEMA, 2018). However, these methods normally do not clearly communicate the

116   mechanisms of flooding for specific locations. In other words, it is not clear if the flooding is caused by

117   the individual or combined impact of storm tide and heavy rainfall. This is problem in part because flood

118   mitigation strategies typically target either rainfall-driven flooding (e.g., stormwater controls) or tidally-

119   driven flooding (e.g., flood walls and tide gates). To access flood risk across coastal landscapes, Bilskie

120   and Hagen (2018) proposed a methodology to delineate coastal floodplains into three flood zones, tidal

121   zone, hydrological zone, and transition zone, according to different driving forces of flooding. The

122   transition zone is defined as an area susceptible the interaction between tidal and rainfall-driven flooding.

123   Application of this method to a flooding event in southeast Louisiana shows that the excess rainfall and

124   storm surge interact nonlinearly and their compound effect is smaller than their superposition (Bilskie and

125   Hagen, 2018). Their study area was primarily located in a rural area with no effect from underground

126   stormwater drainage systems. The transition zone identified from their study is primarily located in a

127   region relatively close to the shoreline, where the tide has a significant impact on flooding. However, in

128   urban environments, the interaction between rainfall-driven flooding and tidal flooding exists on both the

129   land surface and subsurface through stormwater pipeline drainage systems. Thus, the influence of storm

130   tide is not limited to the near-shoreline region, but regions further inland as well.

131   The objective of the study is to develop methodologies to enhance the understanding of the

132   coastal city flood risk and how flood mitigation strategies in improving flood resilience. A high-

133   resolution, coupled 1D pipe/2D overland hydrodynamic model was built using the TUFLOW modeling

134   system for a watershed within the Hague community of Norfolk, VA, USA. TUFLOW solves the full 2D

135   depth averaged momentum and continuity equations for shallow water free surface flow, and incorporates

136   the full functionality of the ESTRY one-dimensional (1D) hydrodynamic network (Syme 2001). This

137   modeling system outputs detailed flooding information on both land surface and underground pipeline

138   system, which allows one to assess flood risk and understand the contribution of flooding from individual

139   or combined factors. The coastal floodplain mapping method proposed in Bilskie and Hagen (2018) was

140   extended for a coastal urban watershed based 2D/1D flood model simulations. The spatial extent of the

141   transition zone was identified using different combinations of storm tide and heavy rainfall events. We

142   also introduce an index to represent the likelihood of a region being susceptible to the combined impact of

143 storm tide and heavy rainfall. The mapping strategy assists in understanding how flood mitigation

144 approcah reduces flooding risk resulting from rainfall and storm tide drivers. The 1D pipe/2D overland

145 flood model is also a powerful tool to evaluate the efficiency of different flood mitigation strategies. As a

146 demonstration, two flood mitigation methods are tested in this study. The methodologies developed in

147 this study can aid city planners and stormwater engineers in other coastal communities to understand and

148 improve flood resilience by targeting both rainfall and storm tide-driven flooding.

149   The remainder of the paper is organized as follows. The methodology section provides

150 background information about the study domain and explains the urban flood model and design the storm

151 scenarios used in the study. It also includes a description of how flood zones were determined within the

152 floodplain mapping analysis and introduces the concept of a transition zone index (TZI). The results and

153 discussion section explains the model evaluation, how the lag between the peak storm tide and rainfall

154 was determined in the modeling scenarios, and flood risk determined by the model. The influence of

155 storm tide on the underground stormwater drainage system is also explored, followed by the coastal

156 floodplain mapping results and a brief exploration of how flood mitigation strategies could reduce the

157 floodplain for the study watershed. The paper concludes with key findings along with possible future

158 research to further advance the approach.

159

160 **2. Methodology**

161 *2.1 Study area*

162 Norfolk, Virginia, USA is the second most populous city in Virginia and the home of world's largest

163 naval base. Norfolk is a highly urbanized and relatively flat community with nearly all areas below

164 elevation 4.5m (North American Vertical Datum of 1988: NADV 88). The relative low elevations and

165 tidal connections to the Chesapeake Bay place a significant percentage of the city at risk of tidal flooding.

166 The tidal flooding risk is more serious under the threat of sea level rise (SLR) and land subsidence (Li et.

167 al., 2013; Sadler et. al., 2017). The study domain is located in the Hague community of the Norfolk, VA

168   (Figure 1). The sources of spatial datasets used in this study are provided in Table 1. The study domain

169   has a total area of 3.7 km^2, including total waterbody area of 0.1 km^2 and land area of 3.6 km^2, in which

170   0.7 km^2 is building area. Ground surface elevation of the study domain varies from 0.3m to 4.2m with an

171   average of 2.6m (NAVD88).

172   Table 1. Spatial Datasets Collected to Build the Urban Flood model

Spatial Dataset	Provider	Sources
LIDAR DEM	VGIN	https://www.vita.virginia.gov/integrated-services/vgin-geospatial-services/elevation---lidar/
Land Cover	VGIN	https://www.vita.virginia.gov/integrated-services/vgin-geospatial-services/land-cover/
Basin Boundaries	Norfolk City	https://www.norfolk.gov/index.aspx?NID=1605
Drainage System	Norfolk City	https://www.norfolk.gov/index.aspx?NID=1605
Building Outlines	VGIN	https://www.arcgis.com/home/item.html?id=994d0afa44c046498f9774613671ce9a
Road Centerlines	VGIN	https://www.vita.virginia.gov/integrated-services/vgin-geospatial-services/transportation/

Note: VGIN: Virginia Geographic Information Network

173   In this study, the tide level data was collected from the Sewells Point station (Station ID:

174   8638610), which is 9.7km away from the domain tidal boundary. This tide gauge has the longest tide

175   level record, dating back to 1927, in Virginia. There is no official rain gauge located inside the study

176   domain. Rainfall data was obtained from two weather stations run by the U.S. National Weather Services

177   (NWS) and two other weather stations run by the Hampton Roads Sanitation District (HRSD) (Figure 1).

178   On average, the NWS and HRSD stations are about 9km and 3km away from the study domain center,

179   respectively. The two NWS weather stations have hourly rainfall data available since 1948 and 1973,

180   respectively. The HRSD stations were installed in January 2016. For hurricane events simulated the

181   study, the NWS rainfall record was used as rainfall input for hurricanes earlier than 2016, and the HRSD

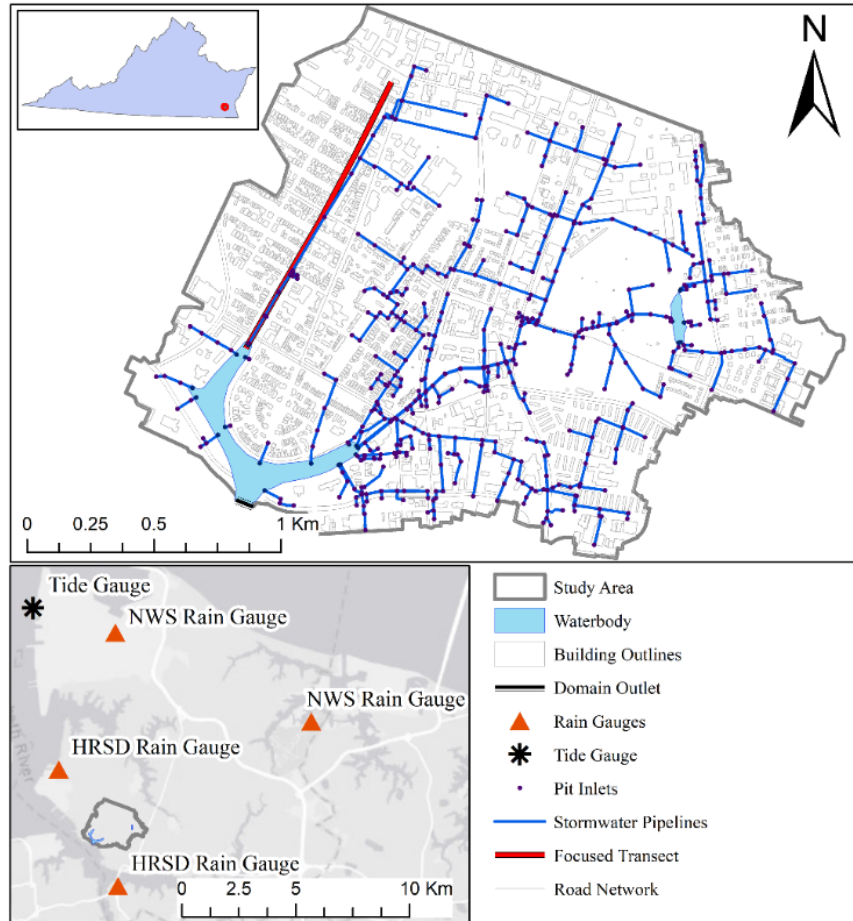182   rainfall record was used for hurricanes after 2016.

183

184   Fig. 1. Study area with tide gauge and rain gauge locations.

185   *2.2 The Urban Flood Model*

186   The study domain is located in a highly urbanized area with complex flow patterns and paths. The

187   interaction between overland flow and pipe flow significantly increases the complexity of flood modeling.

188   To overcome these difficulties, a 1D pipe/2D overland hydrodynamic flood model was built using the

189   TUFLOW model. TUFLOW was chosen due to its capability to represent surface flow on a 2D domain as

190   well as fluvial and pipe network via its 1D functionality and the dynamically link between the two. The

191   TUFLOW High-performance Computing (HPC) engine allows to execute the model on multiple GPU

192   units, which would significantly speed up model simulations.

9

193   The domain boundary was selected from the basin boundaries provided by the City of Norfolk,

194   and adjusted based on a high resolution LiDAR digital elevation model (DEM) and the underground

195   drainage system. There is no rainfall-driven flow, in the form of overland or pipe flow, entering into the

196   study domain from adjacent watersheds. Therefore, all rainfall-driven flooding is generated inside the

197   domain. The outlet of the domain connects to the Elizabeth River, which is a portion of the Chesapeake

198   Bay. Wave speed of tide is currently not considered in this study. So, the tide level at Swells Point was

199   considered to be the same as the outlet of the study watershed. The topography of the 2D domain was

200   defined using a $1m \times 1m$ Lidar DEM, building outlines, and road centerlines collected from the Virginia

201   Geographic Information Network (VGIN), as shown in Table 1. A land cover dataset with 1m spatial

202   resolution was obtained from VGIN to define the overland roughness. The Manning's roughness

203   coefficients for overland flow from McCuen (1998) were assigned to the 2D domain based on the land

204   cover types, as shown in Table 2. For a small watershed, flooding is primarily from short-duration

205   extreme storm events (Bryndal et al., 2017). At the same time, the current study area has an

206   imperviousness ratio of 57% and shallow groundwater level. Thus, infiltration is expected to have minor

207   influence on flooding caused by extreme storm events. Therefore, infiltration was not considered in the

208   current version of the urban flood model, which presumes saturated conditions within the watershed prior

209   to the model simulation period.

210   Table 2. Parameters used in the 1D pipe/2D overland hydrodynamic model

Parameters	Type	Value
Manning's n value of 2D overland surface	Asphalt	0.012
	Concrete	0.013
	Other urban feature	0.012
	Grassland	0.15
	Shrub land	0.4
Manning's n value of 1D pipelines	Plastic pipes	0.012
	Concrete pipe	0.014
	Cast iron pipe	0.013
	Corrugated-metal pipe	0.015
	Brick	0.014

211   TUFLOW solves the full 2D depth averaged momentum and continuity equations for shallow

212   water free surface flow, and incorporates the full functionality of the ESTRY one-dimensional (1D)

213   hydrodynamic network (Syme 2001). In TUFLOW, inlets and grates are represented as pits, which allow

214   modelers to specify a depth-discharge relationship between ponding depth at pits and flow rate entering

215   drainage system. The depth-discharge relationship, controlled by the type and dimension of inlet, defines

216   the flow rate of overland stormwater entering into the pipeline system. The urban drainage design

217   manuals from Federal Highway Administration (2009) and state departments of transportation (e.g.:

218   VDOT, 2017) provide methods to calculate the draining capacity corresponding to the type and

219   dimensional of different inlets. In this study, the depth-discharge curves were determined for different

220   types of inlets based on the VDOT Drainage Manual (2017). The initial pipeline entrance and exit energy

221   loss coefficients are set as value of 0.5 and 1.0, respectively. TUFLOW is capable of automatically

222   adjusting energy loss coefficients associated with the contraction and expansion of flow into and out of a

223   structure according to the approach and departure velocities in the upstream and downstream channels.

224   Details of the energy loss adjustment technique are included in TUFLOW manual (2016) and Tullis and

225   Robinson (2008). The Manning's roughness coefficients were assigned to different types of pipelines, as

226   shown in Table 2.

227   *2.3 Designing of Combined Storm Events*

228   This study focuses on storm tide and heavy rainfall occurring with hurricanes on the Virginia coastline. A

229   summary of the hurricane history of central and eastern Virginia is provided by the National Weather

230   Service (NWS, 2016). Flood risk as a consequence of storm tide and heavy rainfall with the return periods

231   varying from 1 to 100-year are simulated and investigated in this study. Thus, hurricanes, resulted in both

232   storm tide and rainfall with recurrence intervals less than one year for coastal Virginia, were filtered out

233   from the list of hurricanes analyzed in this section. Historical hurricanes with rainfall and tide peak

234   recurrence intervals greater than one year are listed in Table 3. Hourly rainfall data were collected from

235   the NWS weather station 013737 due to it having the longest record in the study region. The Sewells

236   Points station was installed in 1927 to collect tide level data, thus only hurricanes happened after 1927 are

237   listed in Table 3. For the 15 hurricanes with an available rainfall record, the total amount of rainfall varies

238   from 16.8mm to 289.9mm. The minimal and maximum tide peaks are 0.55m and 1.95m (NAVD88),

239   respectively. The rainfall durations of the 15 hurricanes vary from 8 to 77 hours with the median of 22

240   hours. Ten out of the 15 hurricanes have rainfall durations between 16 to 30 hours. Therefore, because

241   rainfall events happening during hurricanes in the Virginia coastal region have average durations of about

242   22 hours. A 24-hour duration was selected as the design rainfall events in this study.

243   Table 3. Historical hurricanes in Virginia with return period of rainfall or storm tide greater than one year.

Year	Storm Event	Rainfall Duration (hrs)	Total Rainfall (mm)	Peak Tide Level (m, NAVD88)
1928	Unnamed	--	--	1.13
1933	Unnamed	--	--	1.95
1936	Unnamed	--	--	1.56
1953	Barbara	--	--	0.83
1960	Donna	22	109.6	1.22
1964	Cleo	24	289.9	0.55
1964	Dora	30	122.0	1.19
1971	Doria	22	78.6	0.61
1985	Gloria	18	143.6	1.04
1986	Charley	16	27.5	1.13
1998	Bonnie	14	92.8	1.20
1999	Floyd	33	166.5	1.29
2003	Isabel	8	16.8	1.91
2004	Charley	15	94.6	0.80
2006	Ernesto	27	256.6	1.19
2011	Irene	27	207.7	1.81
2012	Sandy	77	151.8	1.57
2016	Hermine	20	68.2	1.38
2016	Matthew	21	234.7	1.27

244

245   2.3.1 Designing of Storm Tide Events

246   The annual exceedance probability curves of extreme tide levels for the Sewells Points station were

247   generated by the U.S. National Oceanic and Atmospheric Administration (NOAA)

248   (https://tidesandcurrents.noaa.gov/est/curves.shtml?stnid=8638610). The annual exceedance probability

249 curves of extreme tide levels with 95% confidence intervals are included in the report. The curves were

250 calculated from the annual highest tide levels after the mean sea level trend was removed. The tide levels

251 with different return periods along with the 95% confidence intervals are obtained from the NOAA report

252 as shown in Table 4. The tide level was converted from the Mean Higher High Water (MHHW) datum to

253 NAVD88 to be consistent with the urban flood model settings.

254 Table 4. Annual exceedance probabilities and return periods of extreme tide levels and the matched
255 historical hurricanes.

Exceedance Probability		99% (1-Yr)	10% (10-Yr)	2% (50-Yr)	1% (100-Yr)
Tide Level (m, NAVD88)		0.78	1.56	1.87	2.06
95% Confidence Intervals		0.72 - 0.81	1.35 - 1.61	1.64 - 2.33	1.76 - 2.74
Historical Hurricanes	Name	Charley (2004)	Unnamed (1936)	Isabel (2003)	Unnamed (1933)
	Tide Peak Level (m)	0.8	1.56	1.91	1.95

256

257 The tide level time series observed during historical hurricanes are taken as the references for

258 designing storm tide events. Tide peak levels were selected as an indicator to choose historical hurricanes

259 as reference to design storm tide events. For storm tides with certain return periods in Table 4, the

260 matched hurricane events in Table 3 have tide peak levels that are close to the storm tide peaks and fall in

261 between the 95% confidence intervals. The tide level observations of the matched hurricanes would be

262 taken as the designed storm tide events. Take the 50-year storm tide event as an example. According to

263 Table 4, the 50-year tide has a peak of 1.87m (NAVD88) with 95% confidence intervals from 1.64m to

264 2.33m. In the Table 3, Hurricane Isabel (2003) had a tide level peak of 1.91m, which is closest to the 50-

265 year tide among all these hurricanes. At the same time, the tide peak level of Hurricane Isabel (2003) falls

266 in between the 95% confidence interval of the 50-year tide. Therefore, Hurricane Isabel (2003) was

267 selected as the 50-year storm tide event in this study, and its tide level observation was used to design the

268 50-year storm tide event. Designed storm tide events with return periods of 1, 10, 50, and 100 years are
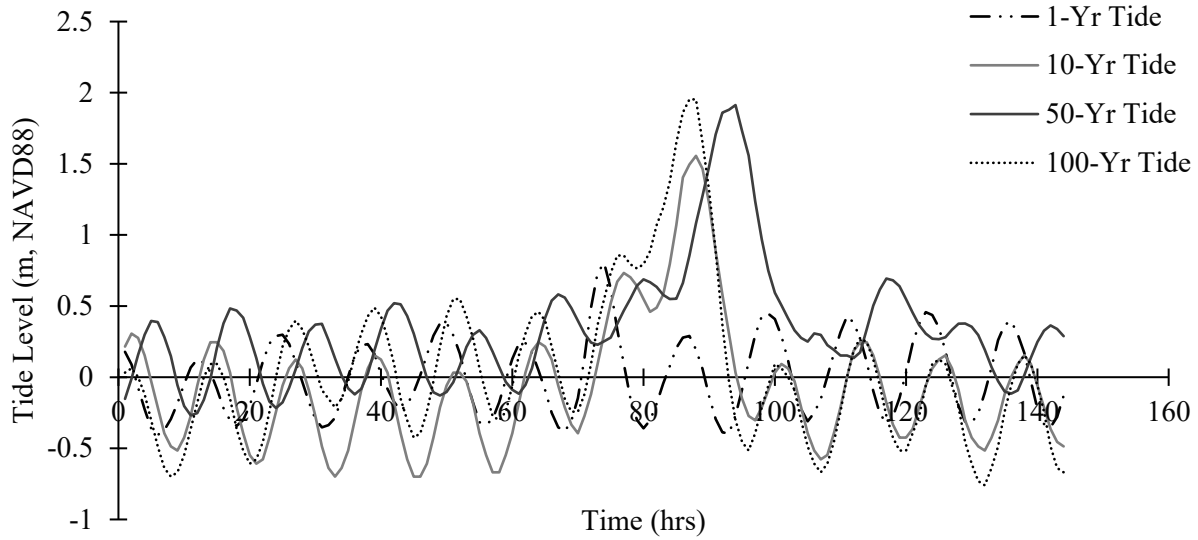
269 presented in Figure 2.

Fig. 2. Designed storm tide events with different return periods.

2.3.2 Designing of Heavy Rainfall Events

In this study, the rainfall intensity-duration-frequency (IDF) curves were obtained from the NOAA Atlas 14 precipitation frequency estimates (Bonnin et. al., 2006). The NOAA Atlas 14 contains precipitation frequency estimates with associated confidence intervals for the United States, and it is provided through a web site (https://hdsc.nws.noaa.gov/hdsc/pfds/pfds_map_cont.html). The 24-hour rainfall intensities with the 90% confidence intervals for different return periods were obtained from the NOAA Atlas 14 and are shown in Table 5.

Table 5. NOAA Atlas 14 precipitation frequency estimates with 90% confidence intervals.

Exceedance Probability	99% (1-Yr)	10% (10-Yr)	2% (50-Yr)	1% (100-Yr)
24-Hr Rainfall Intensity (mm)	74	140	202	234
90% Confidence Intervals (mm)	69 - 81	129 - 152	183 - 218	210 - 253

The rainfall distribution used for rainfall design storms was obtained from a Natural Resources Conservation Service (NRCS) study (Merkel et al., 2015). In Merkel's study (2015), four types of rainfall distributions were developed from data in the NOAA Atlas 14. A map showing a multistate area with groups of regional precipitation distributions was presented along with tables containing 24-hour precipitation distributions in Merkel's study (2015). The current study domain is located in the region of

14

286   Type C precipitation distribution. The precipitation distribution is non-dimensional between values 0 to

287   1.0. Designed rainfall events were generated by multiplying the Type C precipitation distributions with

288   the corresponding 24-hour rainfall intensities from the NOAA Atlas 14. The synthetic rainfall events with

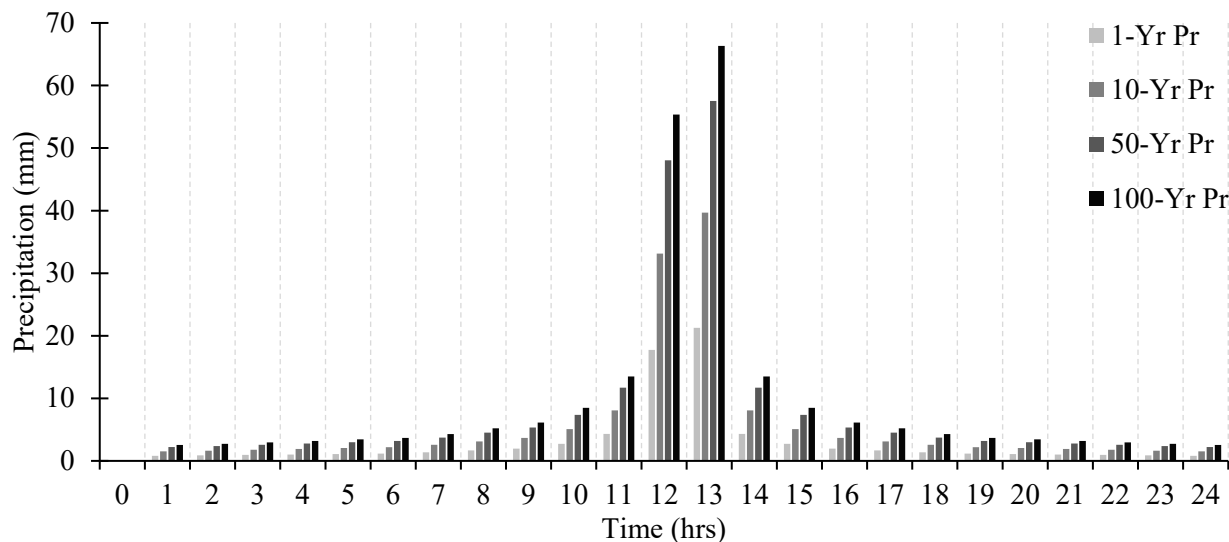289   different return periods are presented in Figure 3.

290
291   Fig. 3. Synthetic 24-hour heavy rainfall events with different return periods.

292   A series of compound storm scenarios were created by combining different synthetic storm tide

293   and heavy rainfall events. The combined impact of storm tide and heavy rainfall are investigated

294   according to the urban flood model simulation for these storm scenarios. Flood simulations on both 2D

295   land area and 1D pipelines were generated as outputs.

296   *2.4 Determine Food Zones*

297   According to Bilskie and Hagen (2018), the coastal floodplain can be separated into three different flood

298   zones, hydrological zone, tidal zone, and transition zone, based on the driving forces of flooding. In the

299   tidal zone, storm tide is the primary factor of flooding and rainfall has negligible impacts. The tidal zone

300   is usually located near a shoreline. The hydrological zone, normally located inland, is dominated by

301   rainfall-driven flooding with only minor impacts from storm tide. The transition zone is where significant

302   interactions exist between rainfall-driven and tidal flooding.

303   These three flood zones for a specific combined storm event are determined by the maximum

304   water level simulations from three designed storm scenarios. In Simulation I, the storm tide is the only

305   input, i.e., no rainfall input. Simulation II consists of heavy rainfall input with a normal tide. Normal tide

306   means an average astronomical tide that cannot cause flooding in the study domain, and its maximum tide

307   level is lower than all drainage pipeline outlets. Simulation III consists of both storm tide and heavy

308   rainfall. Thus, flooding in Simulations I and II is driven by storm tide and rainfall, respectively, and it is

309   driven by the combined effect of storm tide and rainfall in Simulation III. In the tidal zone, rainfall has

310   negligible impacts on flooding; thus, the maximum water level simulation from Simulation III would

311   have minor differences compared to Simulation I even with the existing of rainfall impact. Therefore, the

312   tidal zone is defined as the area where the maximum water level simulations from Simulations I and III

313   have a difference equal to or smaller than 0.01m. In the hydrological zone, storm tide has minor impacts

314   on flooding. Therefore, the maximum water level simulations from Simulation II and III would be fairly

315   close in the hydrological zone. In the current study, the hydrological zone is identified as the area where

316   the maximum water level simulations from Simulation II and III have a difference equal to or smaller

317   than 0.01m. The transition zone is normally located in between the hydrological and tidal zones. In the

318   transition zone, both the maximum water level simulations from Simulation I and II are smaller than

319   Simulation III with a difference greater than 0.01m.

320   The spatial extent of the transition zone varies with the change of storm tide and heavy rainfall

321   combinations. Thus, simply mapping this zone does not fully describe this complex interaction between

322   storm tide and heavy rainfall. In general, a greater tide peak or rainfall intensity would lead to a larger

323   transition zone. For compound storms with higher tide peaks, the tidal zone and transition zone is more

324   likely to extend further inland. Meanwhile, the increase of rainfall intensity would shrink the spatial

325   extent of the tidal zone. To quantify this interaction, we defined the transition zone index (TZI) as

$$TZI = \frac{M}{N} \tag{1}$$

326   where, M is the number of simulations with transition zones sharing a same location, and N is the total

327   number of simulations. TZI can be computed for any watershed based on the simulations from all the

328   compound storm scenarios, as demonstrated in this study. A high TZI locates an area in the watershed

329   where flooding is the product of interactions between storm tide and heavy rainfall. The higher the TZI,

330   the stronger the interaction between these two primarily mechanisms for coastal flooding. TZI helps to

331   identify regions in the watershed that would be impacted by flood mitigation approaches that target either

332   storm tide driven flooding or rainfall driven flooding.

333   **3. Results and Discussion**

334   *3.1 Model Evaluation*

335   Observations of the depth, extent, and duration of flooding in urban coastal landscapes are very rare;

336   however, such data are essential to evaluate the performance of urban flood models (Smith et al., 2012).

337   Data sources, such as photographs taken of flooded areas, newspaper reports and personal interviews,

338   flood information collected from social media, and crow-sourced drone footage, can be converted to

339   inundation information for model evaluation (Smith et al., 2012; Middleton et al., 2014; Fohringer et al.,

340   2015; Loftis et al., 2017). However, these data sources are often sparse and not available for the current

341   study domain. In the current study, the data source used for flood model evaluation is a crowdsourced

342   flood report dataset from the City of Norfolk, VA. This record includes flooded street locations in Norfolk

343   starting from Hurricane Nicole on 30 September 2010 (Salder et al., 2018).

344   In the flood report record, only the date and location of reports were stored instead of the precise

345   time and flood depth. Therefore, the maximum inundation maps on the date when flood locations were

346   reported were compared with the flood report locations as an indication of model performance. During a

347   storm event, stormwater may cause ponding on the most parts of the study domain. Ponding depth is

348   selected as the indicator for inundation area mapping in this study. The inundation maps shown in this

349   paper only include area with ponding depth greater than 0.1 m. This value was selected to distinguish

350   between dry land and flooded locations during storm events. It is assumed that the impact of flood is

351   negligible for flood management purpose when the water depth is smaller than 0.1m.

352   The model performance was evaluated on Hurricanes Irene (2011), Hermine (2016), and Matthew

353   (2016) (Figure 4). If simulated ponding exists in a 20m buffer of a flood reported location, this flood

354   report was assumed to validate the model simulation. All flood reported locations of Hurricanes Irene and

355   Matthew are consistent with the inundated areas from the simulations. During Hurricane Hermine, 25

356   flood locations were reported, and 22 (88%) locations matched with the flood model simulation. The

357   remaining three flood locations are about 250 m away from the shoreline as shown in Figure 4(b). The

358   ponding depth at these three locations varies from 0.05 m to 0.09 m, which is lower than the cutoff depth

359   selected for inundation area mapping. The crowdsourced flood report dataset contains unique and

360   valuable street-level flood information, but there are still limitations of this dataset. As can be expected

361   when using crowd-sourced data, the flood report dataset has an unknown amount of subjectivity and bias

362   because the flood locations are reported by individuals (Sadler et al., 2018). Nonetheless, using the best

363   available information, it is reasonable to suggest that the urban flood model has predictive skill at

364   simulating flooded roads for three different extreme weather events.
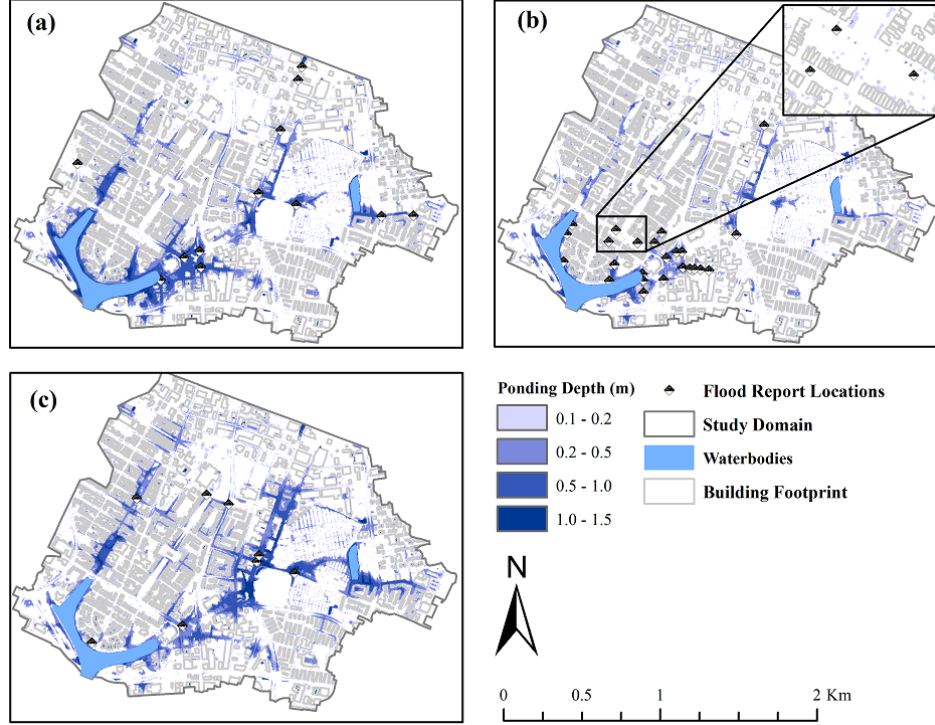
Fig. 4. Ponding depth on time of maximum inundation area and flood report locations for hurricanes (a) Irene (2011), (b) Hermine (2016), and (c) Matthew (2016)

3.2 Time Lag between Storm Tide and Rainfall

The storm scenarios were created by combining the synthetic rainfall and storm tide events; however, we needed a method to match the time axis of rainfall and storm tide events. Usually, there is a time lag between storm tide and rainfall events, and the time lag has a significant impact on flood risk (Zheng et al., 2013). In this section, we show how the time lag between the tide peak and rainfall peak influence flood risk in the study domain.

Time lag is defined as

$$T_{Lag} = T_{Tide\ Peak} - T_{Rainfall\ Peak} \tag{2}$$

where $T_{Tide\ Peak}$ is the time of tide peak and the $T_{Rainfall\ Peak}$ is the time of rainfall peak. In this analysis, the 10-year rainfall is selected as an intermediate rainfall intensity. The 1 and 10-year storm tides were chosen to represent a short duration (less than 6 hours) and a long duration (greater than 6 hours) storm tide, respectively. For each combination of storm tide and heavy rainfall, 17 synthetic storm

19

379   scenarios with time lags varying from -8 to 8 hours were created and simulated. The maximum inundation

380   areas (MIA) in percentage of the total land area and the maximum flood volumes (MFV) on land are

381   shown in Figure 5. The tide levels at the time of rainfall peak for each scenario are provided on the upper

382   row of Figure 5. For both the 1-year tide and 10-year tide cases, the MIAs appear when tide peaks and

383   rainfall peaks happen simultaneously, i.e., time lags equal to zero. The MFVs occur when rainfall peaks

384   are one hour ahead of tide peaks (time lags equal to one). From Figure 5, we found that both MIA and

385   MFV have positive correlations with tide levels at the time of rainfall peaks. When the absolute values of

386   time lag are greater than 4 hours, rainfall peaks happen at low tide periods, and both MIA and MFV are

387   relatively small. For scenarios with absolute values of time lag less than 4 hours, the MIA and MFV

388   increase rapidly with the increase of tide levels at rainfall peaks. Using MIA and MFV as indicators, it the

389   worst flooding appears to happens when the time lags are between -1 to 2 hours. In the current study, the

390   compound storms with simultaneous storm tide and rainfall are chosen to represent the worst-case

391   scenarios, where the worst-case scenarios are determined by using the MIA as the indicator of flood
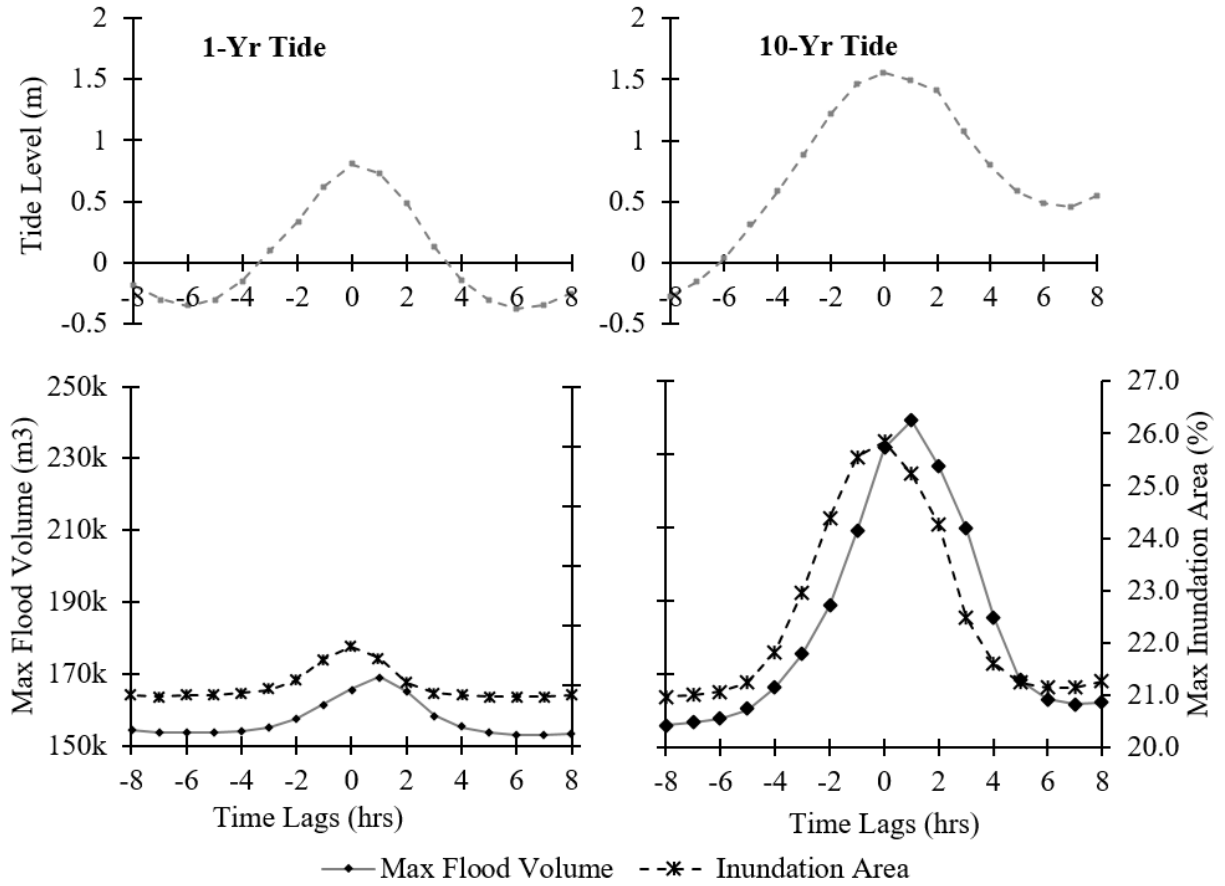
392   severity.

Fig. 5. Influence of time lag between storm tide and rainfall on flood risk with the examples of 10-year rainfall event pairing with 1-year and 10-year storm tide events.

3.3 Flood Risk

The flood ponding depth at the time of maximum inundation area for each storm scenario is presented in Figure 6. Among all storm scenarios, the maximum ponding depth of 1.49 m appeared during the compound storm of 100-year rainfall and 100-year tide. For storm scenarios with fixed rainfall intensity, for example, 1-year rainfall, the inundation area and ponding depth near the shoreline increase rapidly as the storm tide return period increases. Several inland flood-prone areas are isolated from overland tidal flooding; however, for a specific rainfall intensity, both the inundation area and ponding depth in these areas experience a significant increase as the storm tide return period increases. Flooding in these flood-prone areas are greatly influenced by the impact of storm tide on underground pipeline system, which will be discussed in detail in the Section 3.5.

Fig. 6. Combined impact of storm tide and heavy rainfall on flood ponding depth at the time of maximum inundation area.

MIAs and MFVs for different compound storm scenarios are provided in Figure 7. The storm scenario with the 1-year rainfall and 1-year storm tide would flood 12.7% of the land area with a MFV of about $76,000 m^3$. The storm scenario with the 100-year rainfall and 100-year storm tide, according to the model, would cause MIA of 38.9% and MFV of about $457,000 m^3$. From Figure 7, the results show that MIA is more sensitive to the change of rainfall return period compared to tide return period. For example, under the 1-year storm tide condition, MIA increases from 12.7% for 1-year rainfall to 32.1% for 100-year rainfall. In contrast, for the 1-year rainfall event, MIA increases from 12.6% to 22.7% for 1 and 100-

416   year storm tides, respectively. From Figure 7, MFV is susceptible to the change of both rainfall intensity

417   and storm tide severity. The simulations from certain storm scenarios have a similar amount of MIAs or

418   MFVs but different spatial extents. For example, the difference between MIAs for the storm scenario with

419   the 10-year rainfall and 1-year tide and the storm scenario with the 1-year rainfall and 50-year tide is only

420   0.7%. However, Figure 7 shows that these two scenarios, while having a similar MIA, have large

421   differences in the spatial extent of inundated areas. As expected, the flooded area of the event with a 1-

422   year rainfall and 50-year tide is primarily concentrated near the shoreline while the event with 10-year

423   rainfall and 1-year tide has flooded areas more inland with relatively shallow ponding depths.

424
425   Fig. 7. Maximum inundation area in percentage of land area and maximum flood volume on land for
426   different storm scenarios.

427   *3.4 Influence of Storm Tide on Underground Drainage System*

428   The study domain has a complex drainage system, which plays a key role in the stormwater management.

429   Model results and local knowledge of the drainage system both suggest that the efficiency of the drainage

430   system is highly sensitive to the tide levels at the outfalls. During storm tide events, the pipeline outfalls

431   can be partly or even fully submerged. In a submerged state, both the head difference between upstream

432   and downstream pipes and the capacity of the system are reduced, which slows the draining of stormwater

433   through the system.

434   In the study domain, the ground elevation of several roads and streets near the shoreline is higher

435   than surrounding areas. These connected roads and streets form a barrier impeding overland tidal flooding

436   entering into inland regions. The area in between the shoreline and these elevated roads and streets is

437   defined as the shoreline floodplain. Inside the shoreline floodplain, inundation is the combined

438   consequence of overland tidal flooding, local rainfall-driven flooding, and surcharge flow from the

439   underground pipeline system. The inland region is free from overland tidal flooding. Thus, the inundation

440   in the inland region is a consequence of local rainfall-driven flooding and surcharge flow from

441   underground pipelines. Therefore, in the inland region, the flood severity for a fixed rainfall event is

442   determined by the efficiency of the underground pipeline system, which is highly sensitive to the tide

443   levels at outfalls. To explore the relationship between tide level and the efficiency of the drainage system,

444   the flood severity in the inland region is analyzed under the impact of different storm tide events. In this

445   section, the compound storm scenarios with 1-year rainfall and storm tide varying from normal tide to

446   100-year tide were simulated and analyzed. Normal tide means an average astronomical tide that cannot

447   cause flooding in the study domain, and its maximum tide level is lower than all drainage pipeline outlets.

448   As shown in Figure 8, the maximum extent of the shoreline floodplain for these compound storm

449   scenarios are covered by the shoreline floodplain mask, and the inland region is outside the mask. The

450   focus pipes connect the inland region with the shoreline floodplain.
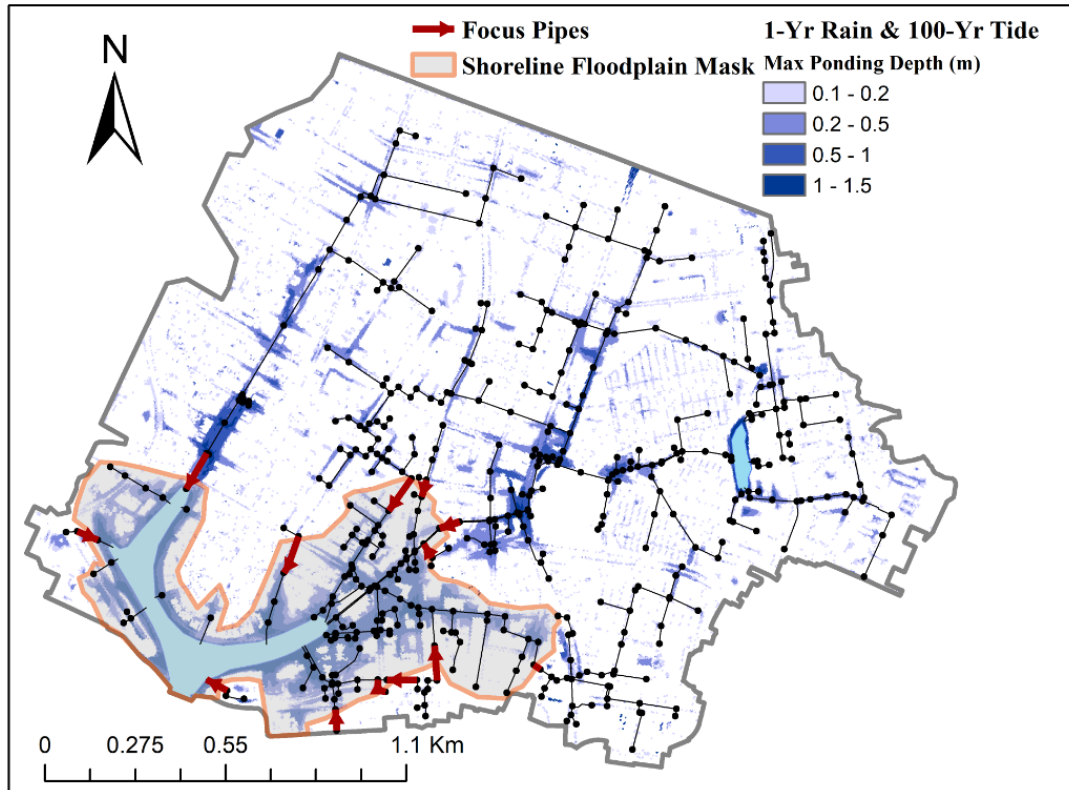
Figure 8. Locations of shoreline floodplain and focus pipes

The time series of total discharge in the focus pipes and the total amount of flood volume in the inland region for the simulated compound storm scenarios are present in Figure 9. From Figure 9 (a), there is no backward flow through the focus pipes under the normal tide and 1-year storm tide conditions. Before hour 12, the total discharge time series have nearly identical trends under these two conditions. However, the peak of total discharge under the 1-year storm tide condition is about 10% lower than the normal tide condition. Meanwhile, from Figure 9 (b), the maximum inland flood volume for the 1-year storm tide is about 5% higher than the normal tide. The pipeline outlets elevation is higher than the normal tide peak, but lower than the 1-year storm tide peak. Therefore, the 1-year storm tide has a blockage effect on the drainage system and would slow down the draining of inland stormwater.

When the recurrence intervals of storm tide are equal to or higher than 10 years, backward flow would occur at the beginning period of the storms. This means these storm tide events are able to reach to the pipelines in the inland region. Under the 10-year tide condition, the total volume of backward flow

25

465   through the focus pipes is $37,000 m^3$. This volume would occupy a large portion of the storage space of

466   pipeline system and slow down the draining of runoff from the inland region. The blockage effect results

467   in the peak of total discharge under the 10-year tide condition decreased by 22% compared to the normal

468   tide condition, and the maximum inland flood volume increased by 34%.

469   The total volumes of backward flow are $310,000 m^3$ and $210,000 m^3$ under the 50 and 100-year

470   storm tide conditions, respectively. In the current paper, designed storm tides are selected based on the

471   peak water levels; for example, the 100-year tide is 0.04m higher than the 50-year tide. However, the

472   duration of the 50-year tide is about 5 hours longer than the 100-year tide, which is the reason that the 50-

473   year tide caused greater volume of backward flow. The water head near the peaks of 50 and 100-year

474   storm tide events are higher than several flood-prone areas in the inland region. Thus, in the simulation, a

475   portion of the backward flow would exit the pipeline system and cause inundation in these areas. From

476   Figure 9 (b), the maximum flood volumes under the 50 and 100-year tide conditions have more than 70%

477   increase compared to the normal tide condition. Therefore, the surcharge flow on top of the blockage

478   effect on pipeline system greatly exacerbate the flooding in inland region.
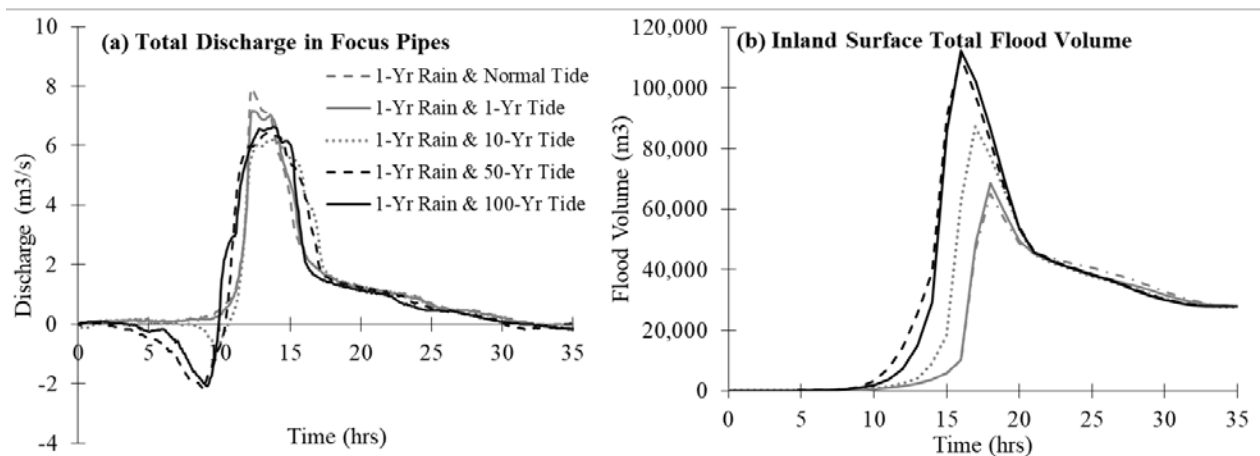

479
480   Figure 9. Influence of tide level on the efficiency of the underground pipeline system: (a) total flood
481   volume of inland area under the condition of different storm tide scenarios; (b) total discharge in focus
482   pipes.

26

483   *3.5 Coastal Floodplain Mapping*

484   The coastal floodplain mapping method is demonstrated by three simulations generated from the

485   50-year rainfall and 50-year storm tide. In Simulation I, the 50-year tide is the only input, i.e., no rainfall.

486   Simulation II consists of 50-year rain and normal tide. Simulation III consists of 50-year rainfall and 50-

487   year tide. For the focused transect in Figure 1, the maximum water level simulations for these three

488   simulations, along with the land surface elevation profile, are presented in Figure 10. In the tidal zone, the

489   maximum water levels from Simulations I and III have a difference less than 0.01m, which means the

490   impact from rainfall is negligible. In the hydrological zone, the difference between maximum water level

491   simulations from Simulations II and III is less than 0.01m. This indicates that storm tide has minor impact

492   in the hydrological zone, and rainfall is the dominating factor. The transition zone is normally located

493   between the tidal zone and hydrological zone. In transition zone, the maximum water level from

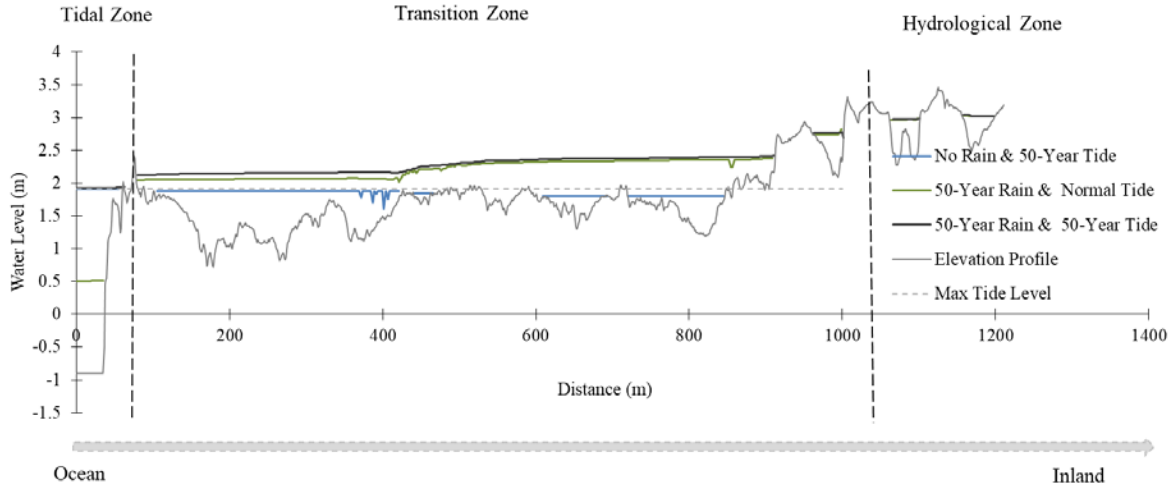494   Simulation III is higher than both Simulations I and II.

495

496 Fig. 10. Land surface elevation profile and simulated maximum water levels across the selected transect for
497 three storm scenarios.

498   For Simulation III, the spatial extent of different flood zones are identified, as shown in Figure 11.

499   The total inundation area is $1.17 km^2$, which is about 32.5% of the land area. The inundation area includes

500   7% of the tidal zone, 43% of the hydrological zone, and 50% of the transition zone. The tidal zone is located

501   in a narrow region near the shoreline. The hydrological zone is primarily distributed in inland region. The

502   transition zone, as originally proposed by Bilskie and Hagen (2018), is located relatively close to the

503   shoreline. However, in this study and in contrast to the Bilskie and Hagen (2018) study, due to the existing

504   of pipeline system, the transition zone can reach to much further inland areas. This is because the strong

505   interaction between rainfall-driven and tidal flooding exists for both the ground surface and underground
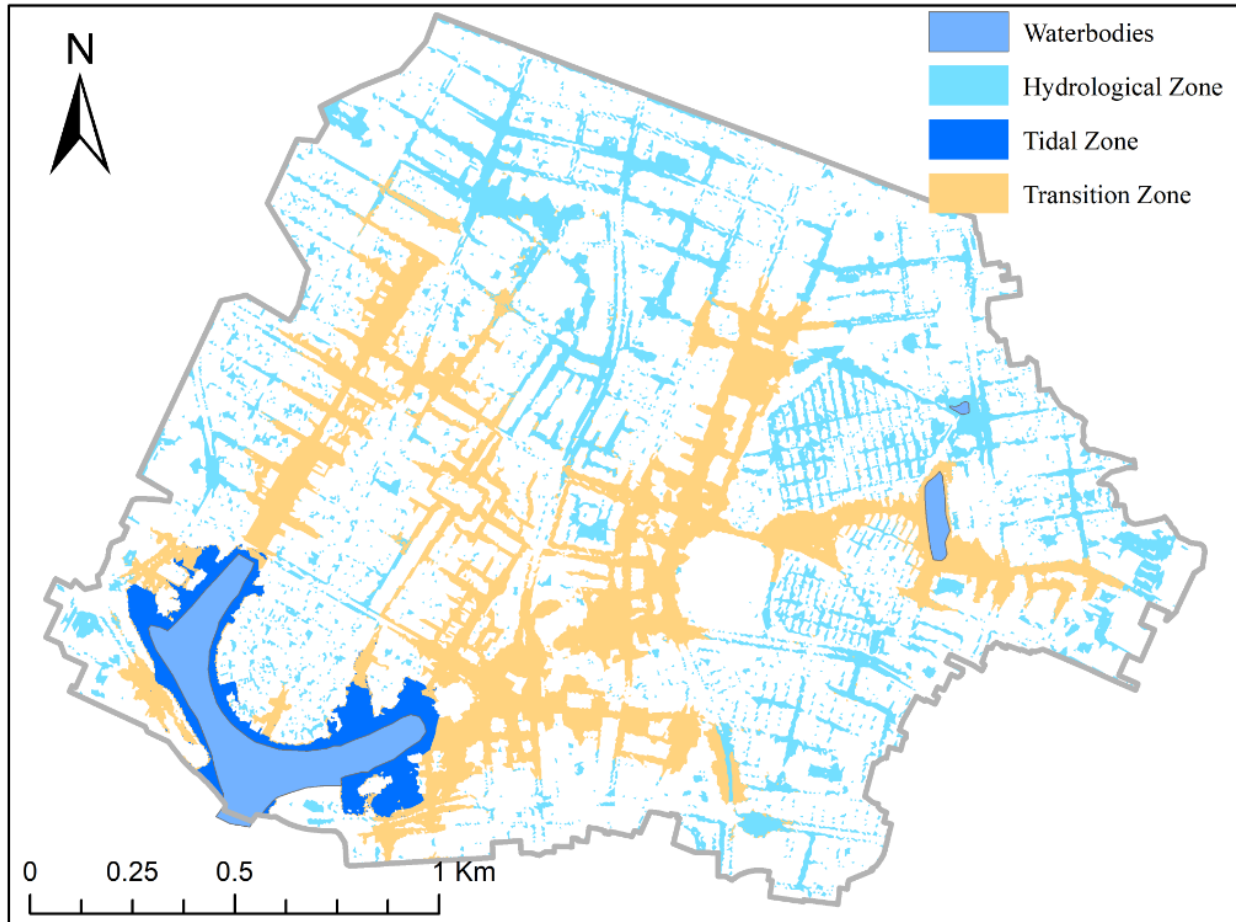
506   drainage systems.

507
508   Fig. 11. Flooding zones identified for storm scenario consists of 50-year storm tide and 50-year heavy
509   rainfall

510   Based on the simulations from the 16 compound storm scenarios in this study, the transition zone

511   index (TZI) was computed and presented in Figure 12. Generally, high TZI locates flood-prone areas

512   where strong interaction exists between storm tide and heavy rainfall. These regions are prone to rainfall-

513   driven flooding due to the relatively low elevation comparing to surround areas. Meanwhile, storm tide

514   would slow down the draining of stormwater from these regions, and in extreme conditions, pipe flow can

515 become surcharge flow and exacerbate flooding severity. The high TZI areas are normally located in the

516 middle region between shoreline and inland area. The inland region has zero or relatively small TZI,

517 which means rainfall is the dominating factor of flooding. Thus, in the inland region, stormwater control

518 measures (e.g., detention pond or rain garden) are effective flood mitigation strategies. In the near-

519 shoreline region, storm tide is the primary driving factor of flooding because of the small TZI. Therefore,

520 tide control measures (e.g., tide gates or flood walls) can be effective to reduce flood risk. For the high

521 TZI areas, both stormwater and tide control measures can potentially help to reduce the flood risk, and the

522 efficiency and mechanisms can be evaluated and explored using the 1D pipe/2D overland flood model.
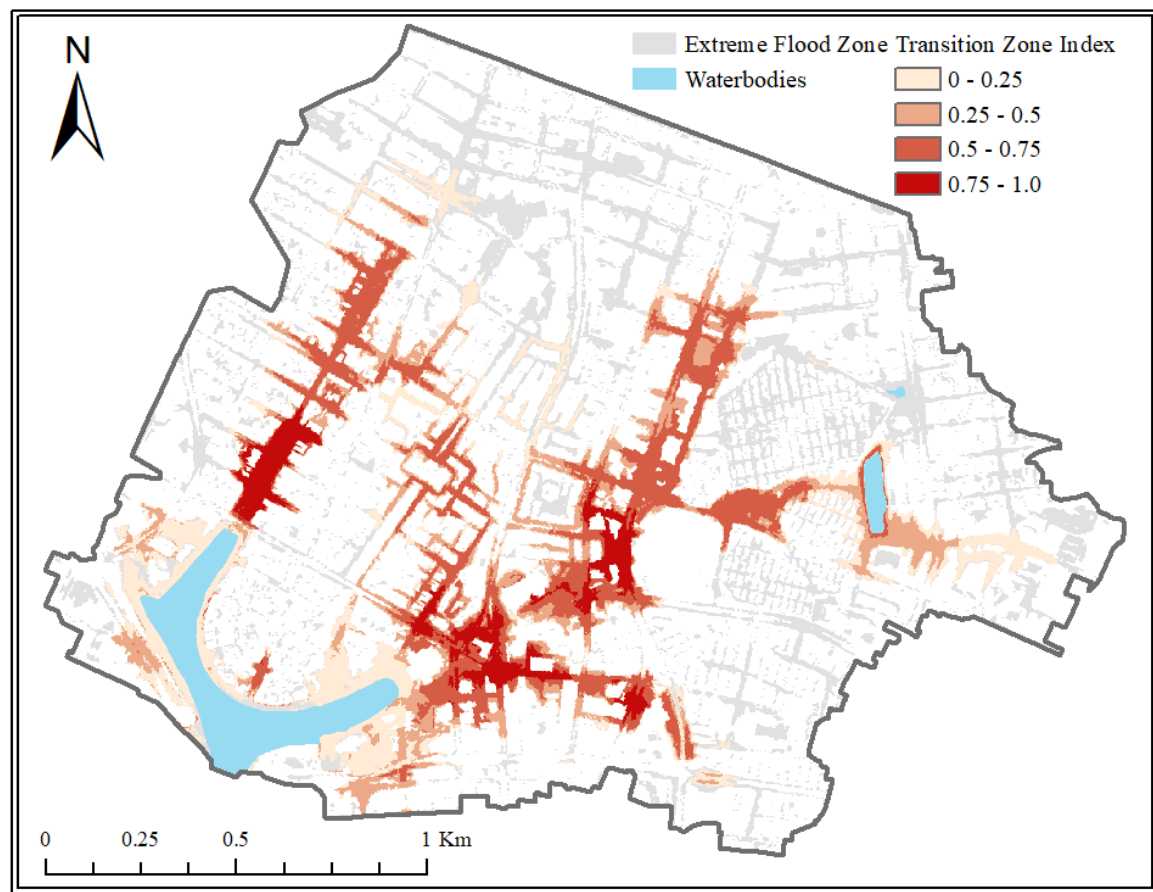

523
524 Fig. 12. Transition zone index estimated based on all compound storm scenario simulations

525 *3.6 Flood Mitigation Strategies*

526 In order to demonstrate how the model can be used to aid decision makers when decided between

527 strategies for improving flood resilience within a system, two mitigation strategies were explored for the

29

528   case study watershed. In both cases, the TZI maps help decisions makers to anticipate regions within the

529   watershed that will be improved based on the mitigation strategy selected. The first strategy is to install

530   flap gates at certain locations within the drainage system to block backflow from high tide. This strategy

531   is aimed at improving flood resilience for areas in the tidal zone with a low TZI value. The second

532   strategy is to increase the useable capacity of a detention pond within the watershed to increase its

533   capability for flood control. This strategy is targeted areas in the Hydrological Zone with low TZI value

534   could be impacted by either of these two mitigation strategies in complex ways. The ponding depth

535   reduction ratio is defined as the criteria for quantifying the improved resilience of the flood mitigation

536   methods. The ponding depth reduction ratio is defined as

$$Ponding\ Depth\ Reduction\ Ratio = \frac{MPD_{Modified} - MPD_{Original}}{MPD_{Original}} \times 100\% \qquad (3)$$

537   Where, the $MPD_{Modified}$ is the maximum ponding depth simulation from the urban flood model

538   including flood mitigation method, and the $MPD_{Original}$ is the maximum ponding depth simulation from

539   the original version of the urban flood model with no flood reduction measure.

540   Two methods of using flap gates are discussed in this section. The first method (Version I) is to

541   install flap gates at the 17 outfalls of the drainage system. However, during extreme high tide, overland

542   tidal flooding can reach to near-shoreline region to inundate several pits and manholes, and sea water

543   would enter into the drainage system through these pits and manholes. The region inundated by overland

544   tidal flooding is defined as the tidal floodplain. To further reduce the volume of backward flow from tide,

545   the second method (Version II) is to install flap gates at all pipes covered by the 100-year tidal floodplain.

546   The Version I and II methods were tested on storm scenarios with 1-year rainfall combined with 10 or

547   100-year storm tide events. The maximum ponding depths were simulated from the urban flood models

548   with and without flap gates. The ponding depth reduction ratio were calculated as shown in Figure 13.

549   Overall, the reduction of maximum ponding depth can be observed from the simulation in several

550   flood-prone regions after flap gates are installed, also flap gates have greater influence for a more extreme

551 storm tide event. Under the combined impact of the 1-year rainfall and 10-year tide event, the Version I

552 method is able to reduce the ponding depth by 2% to 5% for several flood-prone areas, and 5% to 15% in

553 a small portion of these flood-prone area. Under the same event, the Version II method generates large

554 area with a reduction ratio between 5 to 15%. For the storm scenarios with 100-year tide, the ponding

555 depth reduction appear more expansive compared with the 10-year tide. However, the reduction ratio

556 from the Version I method is limited to the range of 2 to 15%, and the majority of that is between 2 to

557 5%. For the Version II method, the maximum ponding depth shows a significant reduction in the

558 upstream flood-prone area. In this case, a large area experiences a ponding depth reduction ratio between

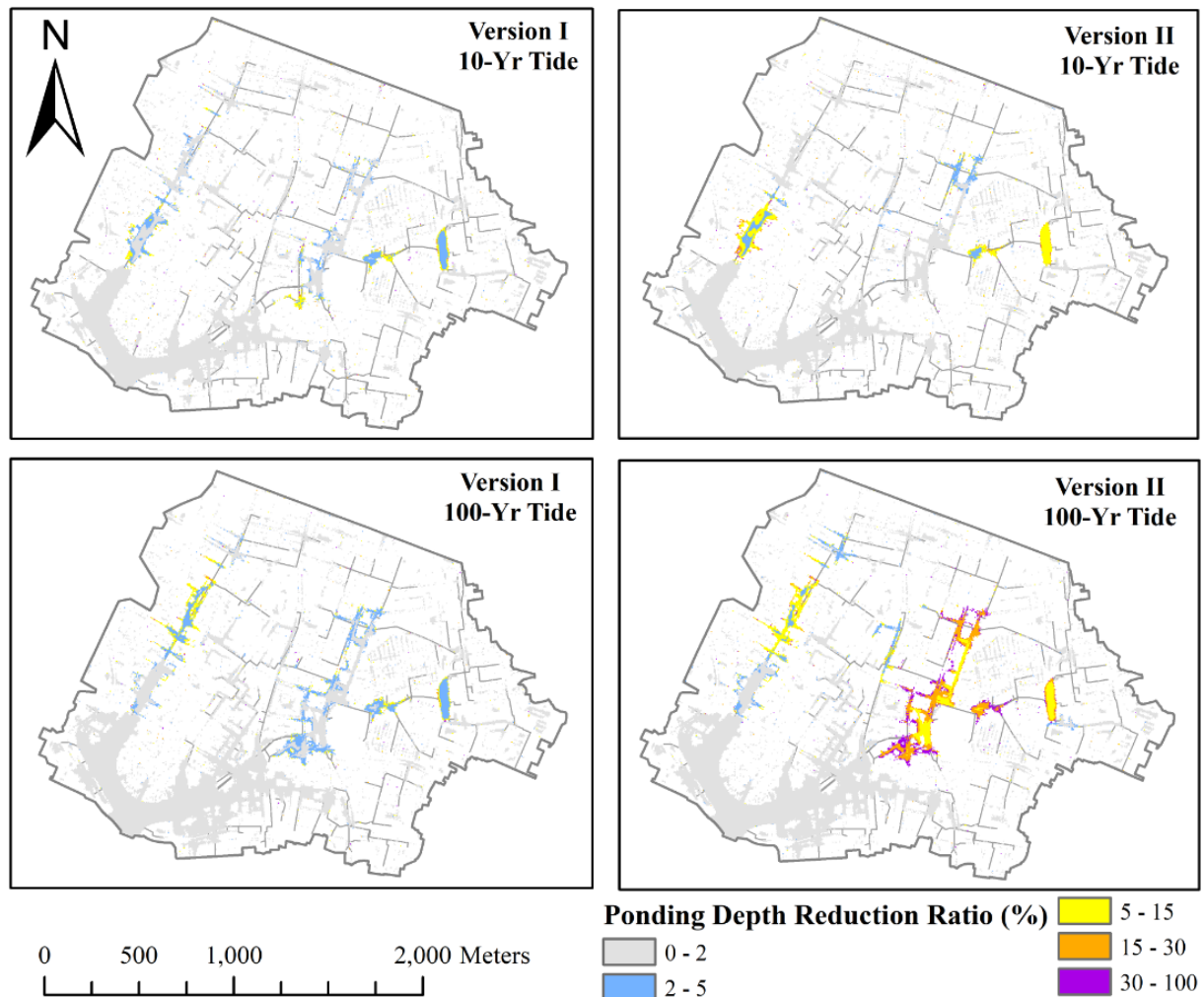559 5 to 30%, and several areas have a reduction ratio greater than 30%.

560

561   Fig. 13. Ponding depth reduction ratio between simulations with and without flap gates: (Version I) flap
562   gates installed at drainage system outfalls; (Version II) flap gates installed in pipes inside the 100-year
563   tidal floodplain. (Tested storm scenarios: 1-year rainfall with 10 and 100-year storm tide events).

564   The detention pond in the study domain is a permanent pool of standing water that provides long-

565   term water quality enhancement of stormwater runoff. Stormwater can also be temporarily stored in the

566   detention pond for downstream flood control. The detention pond has a total capacity of about 24,000m^3

567   and a bed elevation of -1.83m (NAVD88). The detention pond has a normal water level of about 0.35m

568   (NAVD88) and detention storage of about 15,600m^3. The flood control ability of the detention pond is

569   determined by its usable capacity at the beginning of storm events. To enlarge the usable capacity,

570   stormwater control structures can be installed to lower the water level in advance of a forecasted storm.

571   For example, if the water level is lowered to -1m (NAVD88), the detention pond would gain 7,000m^3

572   extra usable capacity for flood control.

573   Two initial water level (IWL) scenarios were tested in this section. For the first scenario (IWL I),

574   the IWL was lowered to -1m above NAVD88. The second scenario (IWL II) had an IWL of -1.83m, the

575   bed elevation, meaning the detention pond is dry under the IWL II condition. The IWL II is tested and

576   discussed to represent a best-case scenario for flood risk reduction. The storm scenarios with the joint

577   occurrences of 1 and 10-year rainfall with 1-year tide are selected to analyze the efficiency of flood

578   mitigation when the detention pond is in IWL I and II conditions.

579   The ponding depth reduction ratios between the maximum ponding depth simulations with

580   lowered IWLs and normal water level of the detention pond are calculated and presented in Figure 14.

581   Generally, lowering the detention pond IWL only influences the flooding in local regions near the pond,

582   and the ponding depth reduction ratios on IWL I and II conditions are very similar for both tested storm

583   scenarios. This is because the usable capacities of the detention pond have relatively small difference

584   (about 2,000m^3) between IWL I and II conditions. With a 1-year rainfall event, the detention pond does

585   not reach to its full capacity under both IWL conditions, and the maximum ponding depths in the region

586   downstream the pond decrease by 2 to 15%. For a 10-year rainfall event, the detention pond does exceed

587   bankfull levels, and the maximum ponding depths in the downstream region near the pond decrease by 5

588   to 15%, and a portion of this region has more than a 15% ponding depth reduction ratio. A 2 to 15%

589   reduction ratio occurs in the further downstream. The most significant flood mitigation appears on the

590   southeastern portion of the detention pond drainage area due to increased capacity to store rainfall runoff
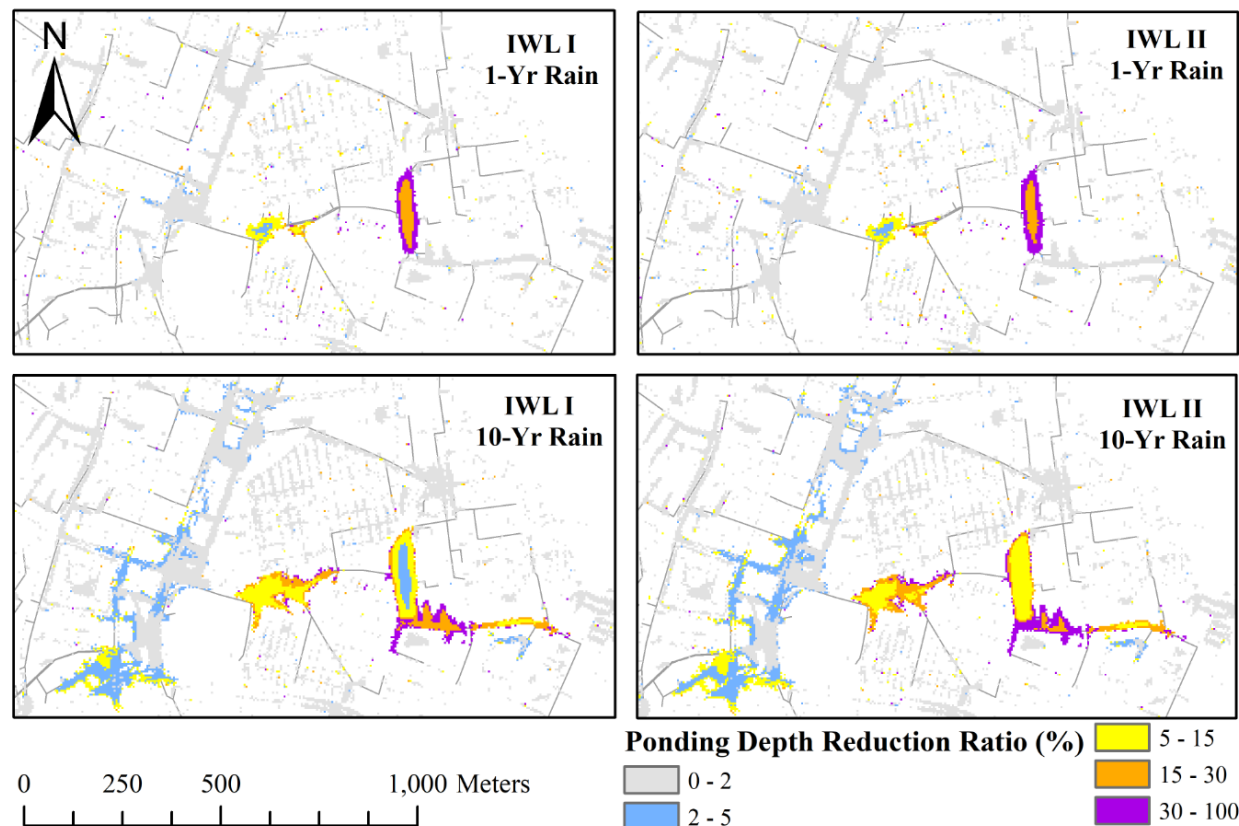
591   generated from this area.

592

593   Fig. 14. Ponding depth reduction ratio between the maximum ponding depth simulations on lowered
594   initial water levels and normal water level of the detention pond: (IWL I) initial water level lower to -1m;
595   (IWL II) initial water level lower to -1.84m. (Tested storm scenarios: 1 and 10-year rainfall with 1-year
596   tide event).

597

598   **4. Conclusions**

599   An overarching objective of this study was to develop methodologies to enhance the understanding of

600   flood risk within coastal urban watersheds. To this end, we modeled how overland flooding in an urban

601   watershed with stormwater drainage infrastructure is affected by storm tide and rainfall events with

602   varying return periods. The study area is located in Norfolk, VA, USA, a city prone to recurrent flooding

33

603   challenge, was the case study system for the study. The 1 to 100-year storm tide events were designed

604   based on storm tides that happened during historical hurricanes impacting the Virginia coastline. A series

605   of rainfall events with return periods varying from 1 to 100-year were designed based on the NOAA Atlas

606   14 precipitation frequency estimates (Bonnin et. al., 2006). These design storm tide and rainfall events

607   were combined to a series of compound storm scenarios. A coupled 1D pipe/2D overland hydrodynamic

608   model was built for the study watershed using the TUFLOW model. The model outputs included detailed

609   flooding information on both land surface and underground pipeline system, which allows to assess flood

610   risk and understand the contribution of flooding from individual or combined factors. Floodplain maps

611   and a new transition zone index (TZI) were created to communicate regions of the watershed under risk

612   of flooding due to tide and rainfall-driven mechanisms. The 1D pipe/2D overland flood model and

613   floodplain visualizations are a powerful tool to evaluate the efficiency of different flood mitigation

614   strategies, as a demonstrated for two flood mitigation methods.

615   Results show how the capacity of stormwater drainage system is highly sensitive to storm tide

616   levels. Based on model simulations, event with a 1-year tide is able to partially submerge the pipeline

617   outlets and has an impact on the pipeline capacity. Storm tide events with return periods greater than or

618   equal to 10 years would significantly reduce the drainage capacity. Extreme storm tide events, for

619   example a 50 and 100-year tide, would cause flooding within the watershed due to the backing-up and

620   day lighting of sea water traveling through stormwater drainage infrastructure. Even for smaller tide

621   events, model simulations show that rainfall driven flooding combined with reduced capacity of the

622   drainage infrastructure caused by tailwater conditions can cause significant flooding in inland regions.

623   Due to the low gradient of the stormwater drainage infrastructure, which is common in many coastal

624   urban areas, this interaction between rainfall-driven flow and sea water flow traveling through the pipe

625   system can influence flooding far into the watershed.

626   This study provides a methodology that can be repeated for other coastal urban watersheds to

627   better understand the influence of storm tide and rainfall-driven flooding through floodplain maps. The

628   coastal floodplain mapping method proposed in Bilskie and Hagen's study (2018) was applied to the

629   urban watershed in the current study. In Bilskie and Hagen's study (2018), the study area is located in a

630   rural area, and the interaction between rainfall-driving and tidal flooding is primarily within the region

631   close to the shoreline. However, in this study, we extended on past work to include the stormwater

632   drainage system, showing that the transition zone can reach much further inland due to the underground

633   stormwater drainage system. The transition zone index (TZI) was defined to represent the likelihood of a

634   location under the impact of strong interaction between tidal and rainfall-driven flooding. In areas with

635   low TZI, flood risk is primarily caused by individual factors. Therefore, flood mitigation measures

636   targeting to individual flood mechanisms can be effective ways to reduce flood risk in these parts of the

637   watershed. For the high TZI areas, both stormwater and tide control measures can potentially assist to

638   reduce the flood risk, and the efficiency and mechanisms can be evaluated and explored using the 1D

639   pipe/2D overland flood model.

640   Lastly, the flood model and floodplain visualization is a powerful tool to evaluate the efficiency

641   of different flood mitigation strategies. As a demonstration, two flood mitigation methods were tested in

642   this study: one targeting rainfall-driven flooding and the second targeting tidal-driven flooding. The

643   model simulations show how both methods would be able to reduce the flood risk for certain flood-prone

644   regions of the watershed. Because the floodplain map helps to visualize regions of the watershed where

645   tide, rainfall, or a combination of these two mechanisms cause flooding, it is easier to see how mitigation

646   strategies improve flood resilience. This methodology can be of a significant value to cities and

647   communities as they work to improve resilience for a host of services that can be impacted by flood risk.

648   The presented model will be used in a future study to explore several aspects of compound storm

649   tide and rainfall-driven flooding. In this study, only tide level data is considered at the boundary as the

650   tide input while tidal flow velocity may have a significant effect on tidal flooding and the function of

651   drainage system. Future research should focus on coupling a hydrodynamic storm surge model with the

652   inland hydrodynamic model to account for these processes. Furthermore, this study is focused on present

653   sea level. However, climate change impacts include increases in rainfall intensity and relative sea level

654   rise (RSLR), which could substantially increase the severity of flood risk in the study area. Future

655   assessments using this model will aim to quantify the impacts of changing climatic conditions on flooding

656   risk.

657

665

666   References

667   Archetti, R., Bolognesi, A., Casadio, A., Maglionico, M., 2011. Development of flood
668   probability charts for urban drainage network in coastal areas through a simplified joint
669   assessment approach. Hydrol. Earth Syst. Sci. 15, 3115–3122. https://doi.org/10.5194/hess-
670   15-3115-2011.

671   Batten, B., Rosenberg, S., Sreetharan, M., 2017. Joint Occurrence and Probabilities of Tides and
672   Rainfall. City of Virginia Beach. https://www.vbgov.com/government/departments/public-
673   works/comp-sea-level-rise/Documents/joint-occ-prob-of-tides-rainfall-4-24-18.pdf.

674   Bilskie, M. V, Hagen, S.C., 2018. Defining flood zone transitions in low-gradient coastal
675   regions. Geophys. Res. Lett. 45, 2761–2770. https://doi.org/https://
676   doi.org/10.1002/2018GL077524.

677   Bonnin, G.M., Martin, D., Lin, B., Parzybok, T., Yekta, M., Riley, D., 2006. NOAA Atlas 14
678   Precipitation-Frequency Atlas of the United States. Silver Spring, Maryland.
679   http://www.nws.noaa.gov/oh/hdsc/PF_documents/Atlas14_Volume2.pdf.

680   Bryndal, T., Franczak, P., Kroczak, R., Cabaj, W., Kołodziej, A., 2017. The impact of extreme
681   rainfall and flash floods on the flood risk management process and geomorphological
682   changes in small Carpathian catchments: a case study of the Kasiniczanka river (Outer
683   Carpathians, Poland). Nat. Hazards 88, 95–120. https://doi.org/10.1007/s11069-017-2858-7

684   Castrucci, L., Tahvildari, N., 2018. Modeling the Impacts of Sea Level Rise on Storm Surge
685   Inundation in Flood-Prone Urban Areas of Hampton Roads, Virginia. Mar. Technol. Soc. J.
686   52, 92–105. https://doi.org/10.4031/MTSJ.52.2.11.

687   Chen, A.S., Evans, B., Djordjević, S., Savić, D.A., 2012. A coarse-grid approach to representing
688   building blockage effects in 2D urban flood modelling. J. Hydrol. 1–16.
689   https://doi.org/10.1016/j.jhydrol.2012.01.007.

690   Dawson, R.J., Speight, L., Hall, J.W., Djordjevic, S., Savic, D., Leandro, J., 2008. Attribution of
691   flood risk in urban areas. J. Hydroinformatics 10, 275.
692   https://doi.org/10.2166/hydro.2008.054.

693   FEMA, 2018. Guidance for flood risk analysis and mapping: coastal general study
694   considerations. https://www.fema.gov/media-library/assets/documents/34953.

695   Fohringer, J., Dransch, D., Kreibich, H., Schröter, K., 2015. Social media as an information
696   source for rapid flood inundation mapping. Nat. Hazards Earth Syst. Sci. 15, 2725–2738.
697   https://doi.org/10.5194/nhess-15-2725-2015.

698   Garcia, R., Restrepo, P., DeWeese, M., Ziemer, M., Palmer, J., Thornburg, J., Lacasta, A., 2015.
699   Advanced GPU paralellization for two-dimensional operational river flood forecasting, in:
700   In 36th International Association for Hydro-Environment Engineering and Research World
701   Congress. The Hague, Netherlands.

702   Hallegatte, S., Green, C., Nicholls, R.J., Corfee-Morlot, J., 2013. Future flood losses in major
703   coastal cities. Nat. Clim. Chang. 3, 802–806. https://doi.org/10.1038/nclimate1979.

704   Hanson, S., Nicholls, R., Ranger, N., Hallegatte, S., Corfee-Morlot, J., Herweijer, C., Chateau, J.,
705   2011. A global ranking of port cities with high exposure to climate extremes. Clim. Change
706   104, 89–111. https://doi.org/10.1007/s10584-010-9977-4.

707   Hunter, N.M., Bates, P.D., Neelz, S., Pender, G., Villanueva, I., Wright, N.G., Liang, D.,
708   Falconer, R.A., Lin, B., Waller, S., Crossley, A.J., Mason, D.C., 2008. Benchmarking 2D
709   hydraulic models for urban flooding. Proc. Inst. Civ. Eng. - Water Manag. 161, 13–30.
710   https://doi.org/10.1680/wama.2008.161.1.13.

711   Huxley, C., Syme, B., 2016. TUFLOW GPU-best practice advice for hydrologic and hydraulic
712   model simulations. in: Proceedings of the 37th Hydrology and Water Resources Symposium
713   (HWRS). Queenstown, New Zealand.

714   Karamouz, M., Razmi, A., Nazif, S., Zahmatkesh, Z., 2017. Integration of inland and coastal
715   storms for flood hazard assessment using a distributed hydrologic model. Environ. Earth
716   Sci. 76, 1–17. https://doi.org/10.1007/s12665-017-6722-6

717   Karamouz, M., F., Zahmatkesh, Z., Goharian, E., S.M., Nazif, S., 2015. Combined Impact of
718   Inland and Coastal Floods : Mapping Knowledge Base for Development of Planning
719   Strategies 141, 1–16. https://doi.org/10.1061/(ASCE)WR.1943-5452.0000497.

720   Li, H., Lin, L., Burks-Copes, K.A., 2013. Modeling of coastal inundation, storm surge, and
721   relative sea-level rise at Naval Station Norfolk, Norfolk, Virginia, U.S.A. J. Coast. Res. 29,
722   18–30. https://doi.org/10.2112/JCOASTRES-D-12-00056.1.

723   Lian, J.J., Xu, K., Ma, C., 2013. Joint impact of rainfall and tidal level on flood risk in a coastal
724   city with a complex river network: A case study of Fuzhou City, China. Hydrol. Earth Syst.
725   Sci. 17, 679–689. https://doi.org/10.5194/hess-17-679-2013.

726   Loftis, J.D., Wang, H., Forrest, D., Rhee, S., Nguyen, C., 2017. Emerging flood model validation
727   frameworks for street-level inundation modeling with StormSense, in: Proceedings of the
728   2nd International Workshop on Science of Smart City Operations and Platforms
729   Engineering. Pittsburgh, PA, pp. 13–18. https://doi.org/10.1145/3063386.3063764.

730   Mark, O., Weesakul, S., Apirumanekul, C., Aroonnet, S. B., and Djordjević, S., 2004. Potential
731   and limitations of 1D modeling of urban flooding. J. Hydrol. (Amsterdam), 299(3–4), 284–
732   299.

733   McCuen, R.H., 1998. Hydrologic Analysis and Design, Second. ed, Prentice Hall. New Jersey.
734   ISBN: 9786468600.

735   Merkel, W.H., Moody, H.F., Quan, Q.D., 2015. Design rainfall distributions based on NOAA
736   Atlas 14 rainfall depths and durations. Beltsville, MD.
737   https://www.wcc.nrcs.usda.gov/ftpref/wntsc/H&H/rainDist/FIHMC_2015_Rainfall_Distrib
738   ution_NOAA_14_Merkel.pdf.

739   Middleton, S.E., Middleton, L., Modafferi, S., 2014. Real-time crisis mapping of natural
740   disasters using social media. Soc. Intell. Technol. 29, 9–17.
741   https://doi.org/10.1109/MIS.2013.126.

742   Morsy, M.M., Goodall, J.L., O'Neil, G.L., Sadler, J.M., Voce, D., Hassan, G., Huxley, C., 2018.
743   A cloud-based flood warning system for forecasting impacts to transportation infrastructure
744   systems. Environ. Model. Softw. 107, 231–244.
745   https://doi.org/10.1016/j.envsoft.2018.05.007.

746   NWS, 2016. The hurricane history of central and eastern Virginia.
747   https://www.weather.gov/media/akq/miscNEWS/hurricanehistory.pdf

748   Ray, T., Stepinski, E., Sebastian, A., Bedient, P.B., 2011. Dynamic modeling of storm surge and
749   inland flooding in a Texas coastal floodplain. J. Hydraul. Eng. 137, 1103–1110.
750   https://doi.org/10.1061/(ASCE)HY.1943-7900.0000398.

751   Sadler, J.M., Goodall, J.L., Morsy, M.M., Spencer, K., 2018. Modeling urban coastal flood
752   severity from crowd-sourced flood reports using Poisson regression and Random Forest. J.
753   Hydrol. 559, 43–55. https://doi.org/10.1016/j.jhydrol.2018.01.044.

754   Sadler, J.M., Haselden, N., Mellon, K., Hackel, A., Son, V., Mayfield, J., Blase, A., Goodall,
755   J.L., 2017. Impact of sea-level rise on roadway flooding in the Hampton Roads Region,
756   Virginia. J. Infrastruct. Syst. 23, 05017006. https://doi.org/10.1061/(ASCE)IS.1943-
757   555X.0000397.

758   Silva-Araya, W.F., Santiago-Collazo, F.L., Gonzalez-Lopez, J., Javier Maldonado-Maldonado,
759   2018. Dynamic modeling of surface runoff and storm surge during hurricane and tropical
760   storm events. Hydrology 5, 1–28. https://doi.org/10.3390/hydrology5010013.

761   Smith, R.A.E., Bates, P.D., Hayes, C., 2012. Evaluation of a coastal flood inundation model
762   using hard and soft data. Environ. Model. Softw. 30, 35–46.
763   https://doi.org/10.1016/j.envsoft.2011.11.008.

764   Svensson, C., Jones, D.A., 2004. Dependence between sea surge, river flow and precipitation in
765   south and west Britain. Hydrol. Earth Syst. Sci. 8, 973–992. https://doi.org/10.5194/hess-8-
766   973-2004.

767   Syme, W.J., 2008. Flooding in Urban Areas-2D Modelling Approaches for Buildings and
768   Fences, in: 9th National Conference on Hydraulics in Water Engineering. Darwin City,
769   Australia, pp. 23–26.

770   Syme, W.J., 2001. TUFLOW–Two & one-dimensional Unsteady FLOW Software for Rivers,
771   Estuaries and Coastal Waters, in: Paper Presented at the IEAust Water Panel Seminar and
772   Workshop on 2d Flood Modelling. Sydney,Australia, pp. 2–9.

773   Upadhyaya, J.K., Biswas, N., Tam, E., 2014. A review of infrastructure challenges: assessing
774   stormwater system sustainability. Can. J. Civ. Eng. 41, 483–492.
775   https://doi.org/10.1139/cjce-2013-0430.

776   Wahl, T., Jain, S., Bender, J., Meyers, S.D., Luther, M.E., 2015. Increasing risk of compound
777   flooding from storm surge and rainfall for major US cities. Nat. Clim. Chang. 5, 1093–
778   1097. https://doi.org/10.1038/nclimate2736.

779   Wang, Y., Colby, J. D., Mulcahy, K. A., 2002. An efficient method for mapping flood extent in a
780   coastal floodplain using Landsat TM and DEM data. International Journal of Remote
781   Sensing. 23 (18), 3681-3696. https://doi.org/10.1080/01431160110114484

782   Woodruff, J.D., Irish, J.L., Camargo, S.J., 2013. Coastal flooding by tropical cyclones and sea-
783   level rise. Nature 504, 44–52. https://doi.org/10.1038/nature12855.

784 Xu, K., Ma, C., Lian, J., Bin, L., 2014. Joint probability analysis of extreme precipitation and
785   storm tide in a coastal city under changing environment. PLoS One 9.
786   https://doi.org/10.1371/journal.pone.0109341.

787 Yazdanfar, Z., Sharma, A., 2015. Urban drainage system planning and design - Challenges with
788   climate change and urbanization: A review. Water Sci. Technol. 72, 165–179.
789   https://doi.org/10.2166/wst.2015.207.

790 Zheng, F., Westra, S., Sisson, S.A., 2013. Quantifying the dependence between extreme rainfall
791   and storm surge in the coastal zone. J. Hydrol. 505, 172–187.
792   https://doi.org/10.1016/j.jhydrol.2013.09.054.

793

794

795

796

797 **Appendix A**

798   The watershed is urbanized and flow has complex patterns and paths through building areas.

799 These buildings dissipate energy by forcing the flow to change its direction and speed. In prior studies,

800 the buildings in the 2D model domain have been represented by increasing the roughness coefficient,

801 blocking out of buildings, applying energy loss coefficient in building areas, and setting the buildings as

802 porous elements (Hunter et. al., 2008; Syme, 2008; Chen et. al., 2012). In this study, one assumption is

803 that no water would enter into buildings during simulations. Therefore, the method of blocking out of

804 buildings is the only satisfactory option based on this assumption. As shown in Figure A1, the areas

805 inside building outlines are deactivated from the 2D domain. To make sure no stormwater from rainfall

806 lost by deactivating the buildings areas, a building representation method is proposed in this study,

807 including three major steps: I) deactivate areas inside building outlines from the 2D domain; II) build

808 polygons that includes groups of buildings; and III) apply the rainfall falling on the building areas to the

809 buffered polygon around each group of buildings. The building roofs are designed to drain rain water

810 rapidly and completely. The assumption behind the building representation method is that rain water can

811 drain out of building roofs without any loss of rain water and no delay time from transferring the water

812   from precipitation to ground. This method is reasonable for the study domain where most of its buildings

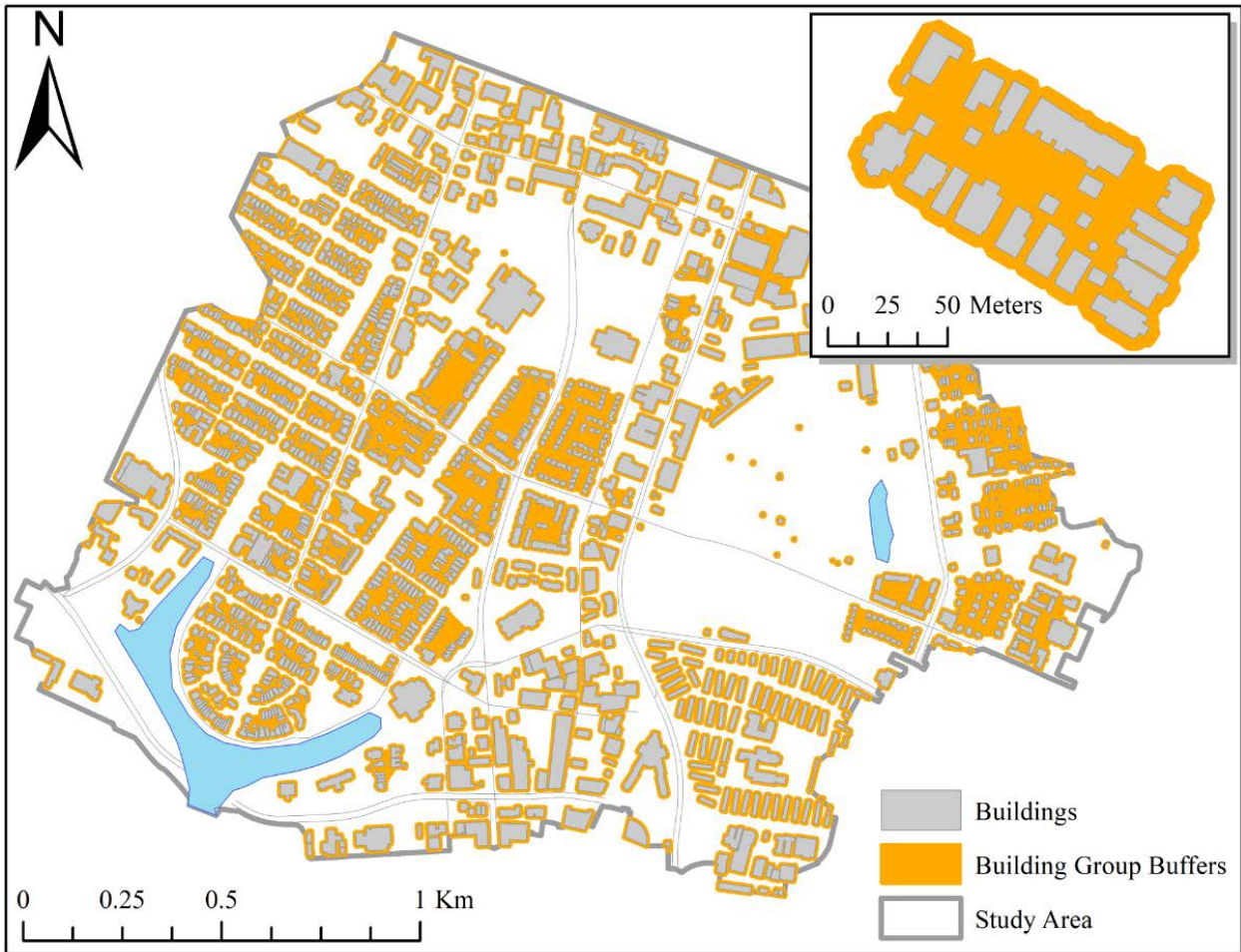813   are residential houses with relatively small roof areas.

814
815   Fig. A1. Representation of buildings in the urban flood model.

816